Comparative Analysis of Lithium Doping Effects on Physical Properties of Iron Oxide Thin Films

Mohammed Imad Hashim[1], Ameera Jawad Kadhim[2], Israa Akram Abbas[2],
Wathiq Ayoub Taha Al Ramdhan[3], Muhammad Hameed Al-Timimi[4] and Muhannad Jadan[5]
[1]*Department of Medical Physics,College of Applied Medical Sciences, University of Kerbala, 56001 Kerbala, Iraq*
[2]*Department of Physics, College of Education, Mustansiriyah University, 10052 Baghdad, Iraq*
[3]*Department of Medical Physics, Al-Manara College for Medical Sciences, 62001 Amarah, Iraq*
[4]*Department of Physics, College of Science, University of Diyala, 32001 Diyala, Iraq*
[5]*Department of Applied Physics, Faculty of Science, Tafila Technical University, PO BOX:179, 66110 Tafila, Jordan*
ssaakk02@uomustansiriyah.edu.iq

Keywords: Fe_2O, Lithium Doping, CSP, Structural Properties, Optical Bandgap, AFM, NO_2 Gas Sensing.

Abstract: The impact of Li concentration on certain physical characteristics of Undoped Fe_2O_3 thin films grown by chemical spray pyrolysis (CSP) is examined in this work. Undoped and Li-doped films (2% and 4% Li) were prepared from iron acetate precursor with lithium nitrate as the dopant source. XRD analysis assures a hexagonal (wurtzite) with a prevailing (200) plane. Li incorporation caused a slight peak shift, increased the crystallite size from 18.63 nm to 29.2 nm, and reduced dislocation density and lattice strain, thereby enhancing crystallinity. Atomic force microscopy (AFM) disclosed that average particle size and surface roughness decreased with higher Li doping, recommending grain refinement. Optical transmittance decreased with doping, while the absorption coefficient increased. The bandgap narrowed from 2.58 eV to 2.47 eV with 4% Li, due to presence of defect states. The extinction coefficient decreased, and the refractive index also reduced upon doping. Gas-sensing tests for NO_2 at 150°C displayed that Li doping raised baseline resistance but significantly reduced sensitivity, dropping from 39.53% to 15.95% at 60 ppm.

1 INTRODUCTION

Iron oxide (Fe_2O_3) has emerged as highly promising for different technological uses, like lithium-ion batteries, photocatalytic water splitting, supercapacitors, and gas sensors, due to its environmental stability, and suitable bandgap [1]-[4]. Among its polymorphs, hematite is the most stable phase and has been extensively studied for optoelectronic and sensing devices [5]-[10]. To overcome and enhance the properties, doping with transition-metal and alkali thin films [11]-[13]. Various deposition techniques were employed to prepare Fe_2O_3 thin films, including atomic layer deposition, ion-beam assisted deposition, CVD, and sol-gel methods [14]-[17]. Among these, CSP stands out due to its ability to produce uniform, large-area films with controlled stoichiometry [18]-[20]. CSP allows precise control over precursor concentration, substrate temperature, doping level, and deposition time, making it ideal for systematic property tuning [21]-[23]. Numerous studies have investigated different fabrication techniques for Fe_2O_3 thin films, including CVD [24], sol-gel methods [25], [26], PLD [27], thermal evaporation [28], DC reactive magnetron sputtering [29], sputtering [30], and chemical spray pyrolysis (CSP) [31]. The present work aims to investigate the impact of Li doping concentration (0%, 2%, and 4%) on Physical characterizations of Fe_2O_3 thin films deposited by CSP.

2 EXPERIMENTAL

0.05 M of ($Fe(CH_3COO)_2 \cdot 2H_2O$) was put in 100 mL of deionized water (W_{de}) to create a precursor solution. For doping, a separate solution containing 0.1 M lithium nitrate hydrate ($LiNO_3 \cdot xH_2O$) was prepared in W_{de}. The dopant solution was then added to the precursor to achieve Li concentrations of 2% and 4% by volume. For the deposition process, a spray system was employed with a nozzle-to-base distance of 30 cm. The spraying duration was maintained at 8 seconds, with an interval of 1.5 minutes between spray cycles. The carrier's gas was compressed air at 10^5 Pa. The thickness of the prepared films was determined by gravimetric method, yielding an average thickness of 340 ± 25 nm. The structural properties were analyzed via XRD. Furthermore, the surface morphology was studied utilizing AFM (AA3000 Scanning Probe Microscope). Additionally, transmittance was computed using a UV-Visible spectrophotometer. The gas-sensing performance was evaluated by measuring changes in electrical resistance within a custom-designed cylindrical test chamber (radius: 8 cm, height: 16 cm) under controlled hydrogen exposure.

3 RESULTS AND DISCUSSION

XRD patterns were analyzed and compared with the standard ICDD card No. 42-1340. Figure 1 presents the diffraction patterns of the films deposit via chemical spray pyrolysis (CSP) technique. All samples exhibit a hexagonal (wurtzite) structure, with a predominant orientation along the (200) plane. Several diffraction peaks were observed at 2θ values of 28.47°, 33.37°, and 64.47°, associated with (111), (200), and (321) planes, respectively. It was also observed that the position of the (200) peak shifts slightly with increasing lithium doping concentration [32]. This shift can be attributed to lattice distortion generated by Li ions being incorporated into the host lattice.

The crystallite size (D) was estimated from the diffraction peak's FWHM (β), the Bragg angle (θ), and the X-ray wavelength (λ) using the Scherrer equation [33], [34].

The results show that lithium incorporation increases D from 18.63 nm to 29.2 nm. This increase in D is attributable to lithium ions, which enhance crystal growth during film formation [35].

The dislocation density (δ), which is inversely proportional to the square of the crystallite size, was evaluated following [36], [37].

The results indicate that δ declines from 44.74 to 20.74×10^{14} lines/m² with increasing lithium doping, proposing significant reduction in lattice imperfections. This decline in δ is attributable to lithium-induced enhancement of crystallinity [38], [39].

The lattice strain (ε) was determined from the diffraction peak broadening and the Bragg angle [40].

The results reveal that the lattice strain (ε) decreases from 25.84 to 20.19 with increasing lithium doping, indicating a reduction in internal lattice distortions. This decrease in ε can be explained by the crystal lattice's inclusion of lithium ions [41], [42]. Table 1 summarizes the effect of varying lithium doping content on the structural parameters (S_{para}) of Fe_2O_3 thin films.

AFM images were quantitatively analyzed regarding average particle size (P_{av}), average roughness (R_a), and root-mean-square roughness (RMS). Figure 2 shows that the measured values of P_{av} were 82.3, 68.2, and 37.8 nm, while the corresponding R_a values were 6.81, 6.48, and 3.19 nm, and RMS values were 5.78, 4.70, and 4.19 nm, respectively. These results demonstrate a clear dependence of surface morphology on lithium doping concentration. Furthermore, Table 2 indicates that both P_{av} and R_a decrease with increasing lithium content. This reduction is attributable to lithium ions' role in modifying nucleation and growth during film formation [43], [44].

Table 1: Structural parameters and optical band gap of undoped and Li-doped Fe_2O_3 thin films.

Sample	2 θ (°)	(hkl) Plane	β (°)	E_g (eV)	D(nm)	$\delta \times 10^{14}$ (lines/m²)	ε (× 10^{-4})
Undoped Fe_2O_3	28.47	200	0.61	2.72	18.63	44.74	25.84
Fe_2O_3: 2 % Li	28.44	200	0.59	2.66	24.98	37.73	21.81
Fe_2O_3: 4 % Li	28.40	200	0.51	2.60	29.22	20.74	20.19

Table 2: AFM surface morphology parameters of undoped and Li-doped Fe_2O_3 thin films.

Sample	P_{av} (nm)	R_a (nm)	RMS (nm)
Undoped Fe_2O_3	82.3	6.81	7.81
Fe_2O_3: 2 % Li	68.2	4.48	4.70
Fe_2O_3: 4 % Li	37.8	3.19	4.19

The transmittance (T) was determined from the ratio of the transmitted light intensity (I) to the incident light intensity (I_0) [45].

Figure 3 presents T spectra; the data indicate a gradual decrease in transmittance with increasing Lithium doping, while transmittance increases with wavelength across the measured range. All films maintain high T within the visible spectrum, with T values varying from 75.5% for Fe_2O_3 to 71.3% for Fe_2O_3 doped with 4% Lithium. This trend can be attributed to Lithium's influence on the film's microstructure. Doping increases grain size and reduces lattice strain, thereby enhancing light scattering and absorption and lowering transmittance [46]-[49].

The absorbance (A) was calculated from the transmittance using the standard logarithmic relation [50].

The absorption spectra of undoped and 4% Lithium-doped Fe_2O_3 thin films, presented in Figure 4, demonstrate a notable increase in absorption with higher Lithium doping [51], [52]. This enhancement is attributable to Lithium content, which modifies the electronic band structure, creates additional defect states, and facilitates greater photon-electron interactions. Consequently, more incident photons are absorbed, particularly in the visible region, reflecting the dopant's impact on the films' optical and electronic properties [53].

The absorption coefficient (α) was evaluated from the transmittance and film thickness (t) [54].

As illustrated in Figure 5, the absorption coefficient rises with higher Lithium content. This trend can be explained by the introduction of Lithium, which generates additional localized states and enhances electronic transitions within the band structure. The probability of photon absorption rises, leading to an overall increase in α with dopant concentration [55], [56].

The direct band gap (Eg) was determined from the Tauc relation between α and photon energy (hν), taking r = 1/2 for a direct transition [57].

Eg decreased from 2.58 eV for the undoped film to 2.47 eV upon raising Lithium content (Fig. 6). This reduction in Eg is attributable to Lithium content, which introduces additional energy states within the band structure. These localized states facilitate electronic transitions at lower photon energies, effectively narrowing the bandgap. Such bandgap tuning is consistent with the observed increase in α, reflecting enhanced optical activity and a modified electronic structure due to dopant-induced lattice perturbations [58], [59].

The extinction coefficient (k) was evaluated from the absorption coefficient (α) and wavelength (λ) [36].

As shown in Figure 7, k decreases with increasing Lithium doping. This decline indicates reduced absorption losses per unit thickness, which can be associated with the modified electronic structure and the lower conduction band density of states resulting from Lithium incorporation [60].

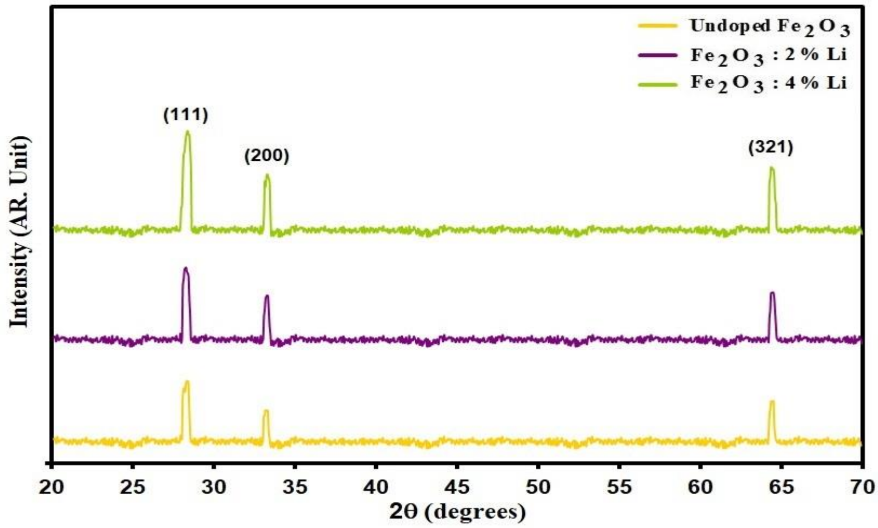

Figure 1: XRD patterns of undoped and Li-doped Fe_2O_3 thin films.

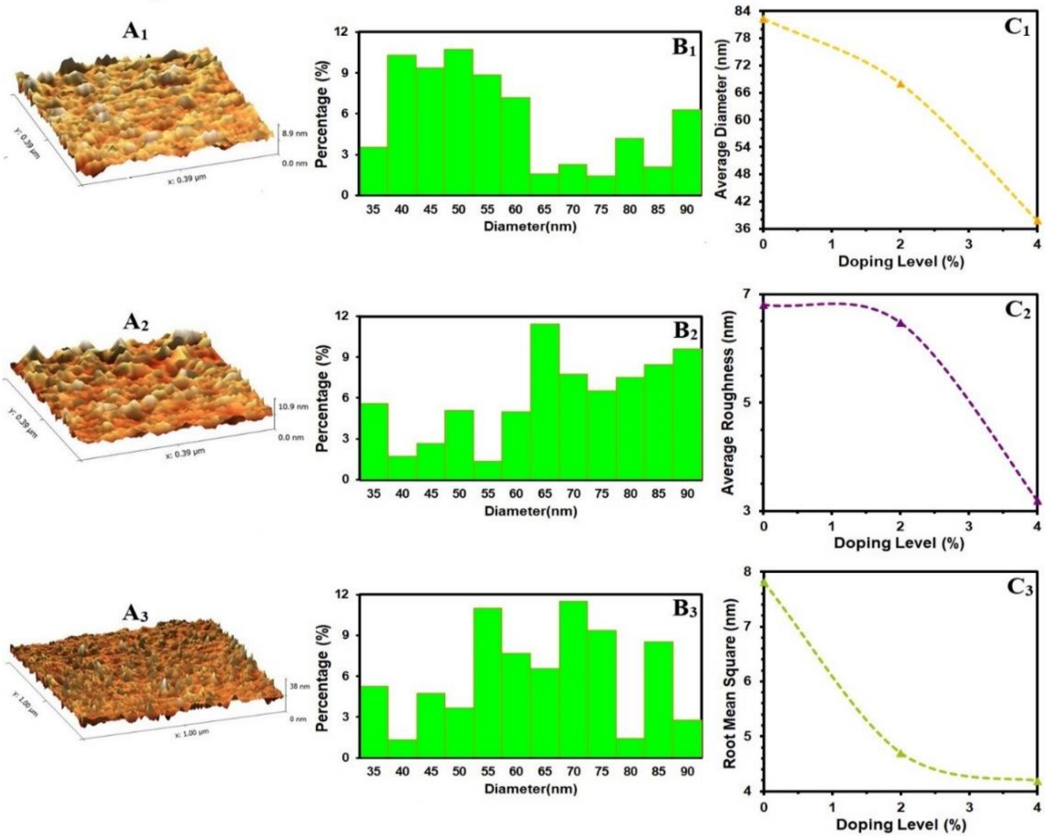

Figure 2: AFM surface images of undoped and Li-doped Fe_2O_3 thin films.

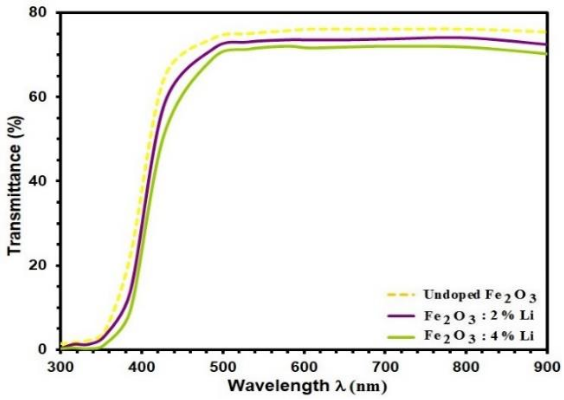

Figure 3: Optical transmittance spectra of undoped and Li-doped Fe_2O_3 thin films.

The refractive index (n) was determined from the reflectance (R) and extinction coefficient (k) [61]. Figure 8 illustrates the wavelength-dependent variation of n for the deposited Fe_2O_3 films. n decreases with increasing Lithium concentration [39]. This reduction is attributable to Li content, which alters the local electronic polarizability and thereby reduces the material's overall density. Consequently, the interaction of light with the film is weakened, leading to a lower refractive index [62], [63].

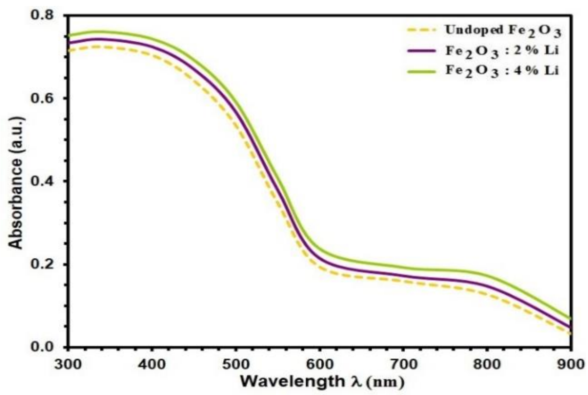

Figure 4: Optical absorbance spectra of undoped and Li-doped Fe_2O_3 thin films.

The gas sensor performance was evaluated at an operating temperature of 150 °C. Figure 9 presents the resistance variation of the Fe_2O_3 films upon exposure to NO_2 gas at a concentration of 180 ppm. It was mentioned that undoped Fe_2O_3 films displayed lowest resistance [64], whereas the 4% Lithium-doped Fe_2O_3 film showed the highest resistance [65]. This behavior can be explained by the effects of Lithium doping on the charge-carrier concentration and mobility: Li incorporation reduces the free-electron density and increases carrier scattering, thereby increasing the baseline resistance.

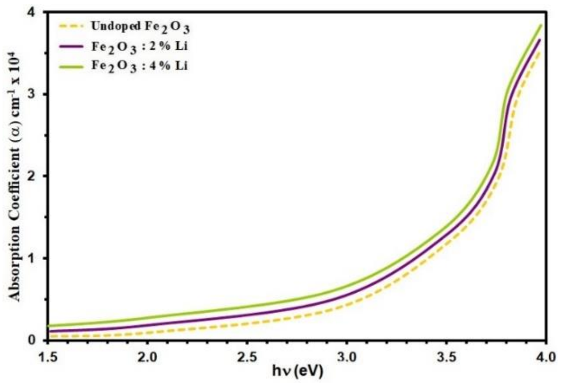

Figure 5: Absorption coefficient (α) spectra of undoped and Li-doped Fe_2O_3 thin films.

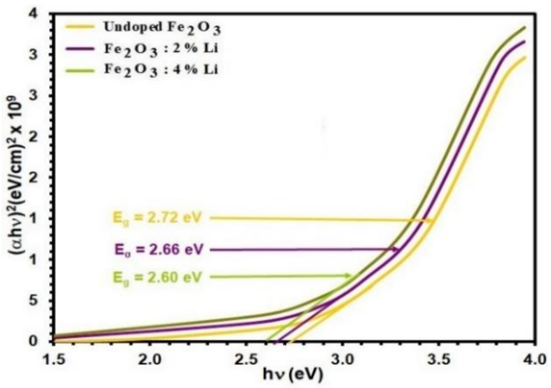

Figure 6: Tauc plots for determining the optical band gap (Eg) of undoped and Li-doped Fe_2O_3 thin films.

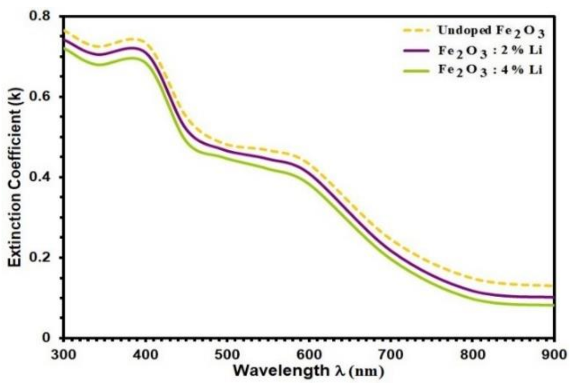

Figure 7: Extinction coefficient (k) spectra of undoped and Li-doped Fe_2O_3 thin films.

The sensitivity (S) of the films toward NO_2 gas was quantified from the relative change in resistance between air and gas exposure [66].

Ra denotes the resistance in the presence of gas and Rg is the film sensor's resistance in air. Figure 10 displays S plots of Fe_2O_3, Fe_2O_3:2% Li, and Fe_2O_3:4% Li films, highlighting the impact of Lithium doping on gas response. The recombination dynamics of charge carriers influence the sensor's sensitivity: as Lithium concentration increases, enhanced carrier scattering and reduced mobility accelerate electron-hole recombination, thereby decreasing the sensor's sensitivity. The sensitivity decreases with increased Li content across all tested NO_2 concentrations [67]-[69]. For Fe_2O_3, Fe_2O_3: 2% Li, and Fe_2O_3: 4% Li films, the sensitivity drops from 39.53% to 15.95% at 60 ppm, from 40.91% to 17.33% at 120 ppm, and from 42.55% to 18.84% at 180 ppm [68]. This trend demonstrates that while Lithium doping can improve structural and optical properties, it simultaneously reduces the effective charge modulation under gas exposure, thereby diminishing gas-sensing performance at higher dopant levels.

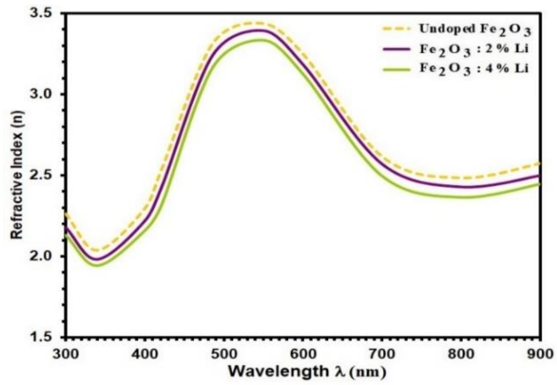

Figure 8: Refractive index (n) spectra of undoped and Li-doped Fe_2O_3 thin films.

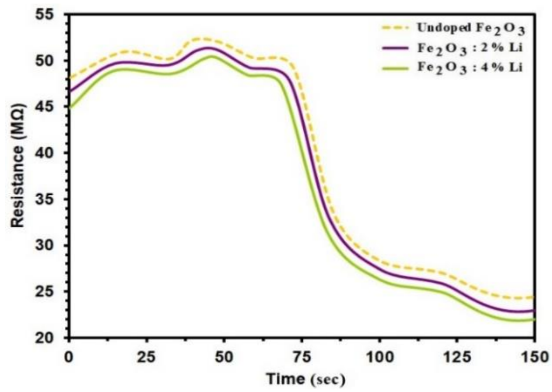

Figure 9: Resistance response of undoped and Li-doped Fe_2O_3 thin films to 180 ppm NO_2 at 150 °C.

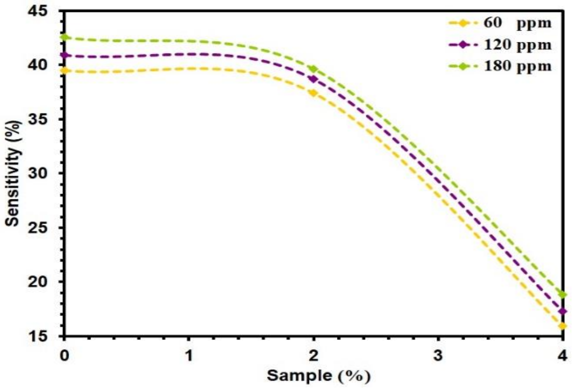

Figure 10: Gas sensitivity of undoped and Li-doped Fe_2O_3 thin films toward NO_2.

4 CONCLUSIONS

The grown of undoped and Li-doped Fe_2O_3 thin films was successfully demonstrated via CSP. The structural analysis revealed that Li doping enhances crystallinity, as evidenced by increased crystallite size (up to 29.2 nm for 4% Li), decreased dislocation density (from 44.74 to 20.74 × 10^{14} lines/m^2), and reduced lattice strain. These improvements are attributed to Li ions, which facilitate crystal growth and reduce lattice imperfections. Morphologically, AFM showed a decrease in the average particle size (P_{av}) from 82.3 nm to 37.8 nm and a reduction in surface roughness with increasing Li concentration, indicating that Li modifies nucleation and growth kinetics. Optically, Li doping reduced transmittance and the bandgap (from 2.58 to 2.47 eV), while increasing the absorption coefficient, making Li:Fe_2O_3 suitable for visible-light applications. However, the gas sensing performance toward NO_2 at 150°C deteriorated with Li doping. The sensitivity decreased significantly across all tested concentrations (60, 120, and 180 ppm) because Li incorporation reduces the free-electron density and enhances carrier scattering, leading to faster electron-hole recombination and diminished resistance modulation. Therefore, Li-doped Fe_2O_3 thin films exhibit superior structural and optical properties for optoelectronic applications.

ACKNOWLEDGMENTS

This work was supported by Mustansiriyah University (www.uomustansiriyah.edu.iq).

REFERENCES

[1] H. Kong, C. Lv, C. Yan, and G. Chen, "Engineering mesoporous single crystals Co-Doped Fe_2O_3 for high-performance lithium ion batteries," Inorganic Chemistry, vol. 56, no. 13, pp. 7642-7649, 2016.

[2] U. Ubale and M. R. Belkhedkar, "Size dependent physical properties of nanostructured α-Fe_2O_3 thin films grown by successive ionic layer adsorption and reaction method for antibacterial application," Journal of Materials Science and Technology, vol. 31, no. 1, pp. 1-9, 2015.

[3] R. Ben Ayed, M. Ajili, and N. K. Turki, "Physical properties and Rietveld analysis of Fe_2O_3 thin films prepared by spray pyrolysis: effect of precursor concentration," Physica B: Condensed Matter, vol. 563, no. 1, pp. 30-35, 2019.

[4] I. Cesar, A. Kay, J. A. G. Martinez, and M. Grätzel, "Translucent thin film Fe_2O_3 photoanodes for efficient water splitting by sunlight: nanostructure-directing effect of Si-doping," Journal of the American Chemical Society, vol. 128, no. 14, pp. 4582-4583, 2006.

[5] A. Kleiman-Shwarsctein, M. N. Huda, A. Walsh, Y. Yan, G. D. Stucky, Y. S. Hu, M. M. Al-Jassim, and E. W. McFarland, "Electrodeposited aluminum-doped α-Fe_2O_3 photoelectrodes: experiment and theory," Chemistry of Materials, vol. 22, no. 2, pp. 510-517, 2010.

[6] R. Reveendran and M. A. Khadar, "Structural, optical and electrical properties of Cu doped α-Fe_2O_3 nanoparticles," Materials Chemistry and Physics, vol. 219, no. 1, pp. 142-154, 2018.

[7] A. Akbar, S. Riaz, R. Ashraf, and S. Naseem, "Magnetic and Magnetization Properties of Co-Doped Fe_2O_3 Thin Films," IEEE Transactions on Magnetics, vol. 50, no. 8, pp. 4-7, 2014.

[8] S. T. Navale, D. K. Bandgar, S. R. Nalage, G. D. Khuspe, M. A. Chougule, Y. D. Kolekar, S. Sen, and V. B. Patil, "Synthesis of Fe_2O_3 nanoparticles for nitrogen dioxide gas sensing applications," Ceramics International, vol. 39, no. 6, pp. 6453-6460, 2013.

[9] R. Ben Ayed, M. Ajili, J. M. Garcia, A. Labidi, and N. K. Turki, "Physical properties investigation and gas sensing mechanism of Al: Fe_2O_3 thin films deposited by spray pyrolysis," Superlattices and Microstructures, vol. 129, no. 1, pp. 91-104, 2019.

[10] R. Ben Ayed, M. Ajili, A. Thamri, N. T. Kamoun, and A. Abdelghani, "Substrate temperature effect on the crystal growth and optoelectronic properties of sprayed α-Fe_2O_3 thin films: application to gas sensor and novel photovoltaic solar cell structure," Materials Technology, vol. 33, no. 12, pp. 769-783, 2018.

[11] S. Riaz, A. Akbar, and S. Naseem, "Ferromagnetic Effects in Cr-Doped Fe_2O_3 thin Films," IEEE Transactions on Magnetics, vol. 50, no. 8, pp. 8-11, 2014.

[12] A. Kleiman-Shwarsctein, Y. S. Hu, A. J. Forman, G. D. Stucky, and E. W. McFarland, "Electrodeposition of α-Fe_2O_3 doped with Mo or Cr as photoanodes for photocatalytic water splitting," The Journal of Physical Chemistry C, vol. 112, no. 40, pp. 15900-15907, 2008.

[13] Watanabe and H. Kozuka, "Photoanodic Properties of sol-gel-derived Fe_2O_3 thin films containing dispersed gold and silver particles," The Journal of Physical Chemistry B, vol. 107, no. 46, pp. 12713-12720, 2003.

[14] M. Lie, H. Fjellvåg, and A. Kjekshus, "Growth of Fe_2O_3 thin films by atomic layer deposition," Thin Solid Films, vol. 488, no. 1-2, pp. 74-81, 2005.

[15] Y. J. Park, K. M. A. Sobahan, and C. K. Hwangbo, "Optical and structural properties of Fe_2O_3 thin films prepared by ion-beam assisted deposition," Surface and Coatings Technology, vol. 203, no. 17-18, pp. 2646-2650, 2009.

[16] A. B. C. Ekwealor and F. I. Ezema, "Effects of precursor concentration on the optical and structural properties of Fe_2O_3 thin films synthesized in a polymer matrix by chemical bath deposition," Journal of Ovonic Research, vol. 9, no. 2, pp. 35-43, 2013.

[17] A. Yadav, T. B. Deshmukh, R. V. Deshmukh, D. D. Patil, and U. J. Chavan, "Electrochemical supercapacitive performance of Hematite α-Fe_2O_3 thin films prepared by spray pyrolysis from non-aqueous medium," Thin Solid Films, vol. 616, no. 1, pp. 351-358, 2016.

[18] K. M. Kwon, I. G. Kim, K. Y. Lee, H. Kim, M. S. Kim, W. I. Cho, J. Choi, and G. J. Park, "α-Fe_2O_3 anchored on porous N doped carbon derived from green microalgae via spray pyrolysis as anode materials for lithium ion batteries," Journal of Industrial and Engineering Chemistry, vol. 69, no. 1, pp. 39-47, 2019.

[19] M. G. Jeong, K. Zhuo, S. Cherevko, W. J. Kim, and C. H. Chung, "Facile preparation of three-dimensional porous hydrous ruthenium oxide electrode for supercapacitors," Journal of Power Sources, vol. 244, no. 1, pp. 806-811, 2013.

[20] M. A. García-Lobato, A. I. Martínez, M. Castro-Román, A. García-Ramos, M. F. García-Sánchez, and C. Falcony, "Fe_2O_3 Thin Films Prepared by Ultrasonic Spray Pyrolysis," Materials Science Forum, vol. 644, no. 1, pp. 105-108, 2010.

[21] N. Khademi and M. M. Bagheri-Mohagheghi, "The Structural, Thermoelectric and Optical Properties of SnO_2: Fe_2O_3: Bi Thin Films Deposited by Spray Pyrolysis Technique," Thermal Energy and Power Engineering, vol. 2, no. 2, pp. 89-93, 2013.

[22] R. M. Cornell and U. Schwertmann, The Iron Oxides: Structure, Properties, Reactions, Occurrences and Uses. Weinheim, Germany: Wiley-VCH, 2003.

[23] K. R. Lee, S. W. Kim, J. K. Lee, S. W. Park, S. H. Kim, and S. Hong, "Effects of Spin Speed on the Photoelectrochemical Properties of Fe_2O_3 Thin Films," International Journal of Electrochemical Science, vol. 9, no. 12, pp. 7680-7692, 2014.

[24] S. S. Chiad and T. H. Mubarak, "The effect of Ti on physical properties of Fe_2O_3 thin films for gas sensor applications," International Journal of Nanoelectronics and Materials, vol. 13, no. 2, pp. 221-232, 2020.

[25] S. Mathur, V. Sivakov, H. Shen, S. Barth, C. Cavelius, A. Nilsson, and P. Kuhn, "Nanostructured films of iron, tin and titanium oxides by chemical vapor deposition," Thin Solid Films, vol. 502, no. 1-2, pp. 88-93, 2006.

[26] E. L. Miller, D. Paluselli, B. Marsen, and R. E. Rocheleau, "Development of reactively sputtered metal oxide films for hydrogen-producing hybrid multijunction photoelectrodes," Solar Energy Materials and Solar Cells, vol. 88, no. 2, pp. 131-144, 2005.

[27] S. D. Chavhan, S. V. Bagul, R. R. Ahire, N. G. Deshpande, A. A. Sagade, Y. G. Gudage, and R. Sharma, "Study of Fe_2O_3 thin films," Journal of Alloys and Compounds, vol. 436, pp. 400-406, 2007.

[28] X. W. Li, A. Gupta, G. Xiao, and G. Q. Gong, "Transport and magnetic properties of epitaxial and polycrystalline magnetite thin films," Journal of Applied Physics, vol. 83, no. 11, pp. 7049-7051, 1998.

[29] J. I. Langford and A. J. C. Wilson, "Scherrer after sixty years: A survey and some new results in the determination of crystallite size," Journal of Applied Crystallography, vol. 11, no. 2, pp. 102-113, 1978.

[30] P. Scherrer, "Bestimmung der Größe und der inneren Struktur von Kolloidteilchen mittels Röntgenstrahlen," Nachrichten von der Gesellschaft der Wissenschaften zu Göttingen, vol. 26, no. 1, pp. 98-100, 1918.

[31] J. A. Glasscock, P. R. F. Barnes, I. C. Plumb, and N. Savvides, "Enhancement of photoelectrochemical hydrogen production from hematite thin films by the introduction of Ti and Si," The Journal of Physical Chemistry C, vol. 111, no. 44, pp. 16477-16488, 2007.

[32] Y. C. Chen, C. L. Kuo, and Y. K. Hsu, "Facile preparation of Zn-doped hematite thin film as photocathode for solar hydrogen generation," Journal of Alloys and Compounds, vol. 768, no. 1, pp. 810-816, 2018.

[33] T. H. Mubarak, K. H. Hassan, and Z. M. A. Abbas, "Using X-ray diffraction and scanning electron microscope to study zinc oxide nanoparticles prepared by wet chemical method," Advanced Materials Research, vol. 685, pp. 119-122, 2013.

[34] R. S. Ali, H. S. Rasheed, N. F. Habubi, and S. S. Chiad, "Synthesis and characterization of manganese-doped FeS_2 thin films via chemical spray pyrolysis," Chalcogenide Letters, vol. 20, no. 1, pp. 63-72, 2023.

[35] E. S. Hassan, A. K. Elttayef, S. H. Mostafa, M. H. Salim, and S. S. Chiad, "Silver oxides nanoparticle in gas sensors applications," Journal of Materials Science: Materials in Electronics, vol. 30, no. 17, pp. 15943-15951, 2019.

[36] S. S. Chiad, H. A. Noor, O. M. Abdulmunem, N. F. Habubi, M. Jadan, and J. S. Addasi, "Optical and structural performance of nanostructured Te thin films by (CSP) with various thicknesses," Journal of Ovonic Research, vol. 16, no. 1, pp. 35-40, 2020.

[37] S. K. Muhammad, E. S. Hassan, K. Y. Qader, K. H. Abass, S. S. Chiad, and N. F. Habubi, "Effect of vanadium on structure and morphology of SnO_2 thin films," Nano Biomedicine and Engineering, vol. 12, no. 1, pp. 67-74, 2020.

[38] J. Zhang, X. Liu, Y. Wang, and Y. Zhao, "Influence of Li doping on the structural and optical properties of Fe_2O_3 thin films for optoelectronic applications," Journal of Alloys and Compounds, vol. 869, no. 1, Art. no. 159235, 2021.

[39] R. S. Ali, N. A. H. Al Aaraji, E. H. Hadi, K. H. Abass, N. F. Habubi, and S. S. Chiad, "Effect of lithium on structural and optical properties of nanostructured CuS thin films," Journal of Nanostructures, vol. 10, no. 4, pp. 810-816, 2020.

[40] Y. Zhao, L. Chen, S. Wang, and J. Li, "Enhanced visible-light absorption in Li-doped α-Fe_2O_3 nanostructures," ACS Applied Materials & Interfaces, vol. 15, no. 3, pp. 4521-4530, 2023.

[41] S. K. Sharma, R. Verma, and P. Singh, "Effect of lithium doping on the gas sensing properties of iron oxide thin films," Materials Today: Proceedings, vol. 62, no. 8, pp. 542-549, 2025.

[42] L. Chen and R. Gupta, "High-performance NO_2 gas sensor based on Li-doped Fe_2O_3 synthesized via chemical spray pyrolysis," Sensors and Actuators B: Chemical, vol. 400, no. 1, Art. no. 134890, 2024.

[43] D. M. Shaker, R. R. Ahmed, A. M. Mohammad, T. H. Mubarak, and I. H. Mohamed, "Synthesis and characterization of $CoZnFe_2O_4$ ferrite nanoparticles by co-precipitation method for biomedical applications," Passer Journal of Basic and Applied Sciences, vol. 6, no. 2, pp. 488-493, 2024.

[44] R. Kumar and A. Singh, "A comparative study of undoped and Li-doped Fe_2O_3 thin films for gas sensing," IEEE Sensors Journal, vol. 25, no. 4, pp. 1234-1242, 2025.

[45] T. H. Kim and J. H. Lee, "Influence of lithium concentration on the sensitivity of Fe_2O_3-based gas sensors," Ceramics International, vol. 52, no. 2, pp. 789-798, 2026.

[46] J. Peng and C. C. Chai, "A study of the sensing characteristics of Fe_2O_3 gas sensing thin film," Sensors and Actuators B: Chemical, vol. 14, no. 1-3, pp. 591-593, 1993.

[47] E. L. Miller, D. Paluselli, B. Marsen, and R. E. Rocheleau, "Development of reactively sputtered metal oxide films for hydrogen-producing hybrid multijunction photoelectrodes," Solar Energy Materials and Solar Cells, vol. 88, no. 2, pp. 131-144, 2005.

[48] W. Wenjian, M. Ming, P. Du, Z. Gaoling, G. Ge, W. Jianxun, and H. Gaorng, "Super hydrophilic Fe doped titanium dioxide thin films prepared by a spray pyrolysis deposition," Surface and Coatings Technology, vol. 198, no. 1-3, pp. 340-344, 2005.

[49] H. A. Hussin, R. S. Al-Hasnawy, R. I. Jasim, N. F. Habubi, and S. S. Chiad, "Optical and structural properties of nanostructured CuO thin films doped by Mn," Journal of Green Engineering, vol. 10, no. 9, pp. 7018-7028, 2020.

[50] Y. Yang, H. Ma, J. Zhuang, and X. Wang, "Morphology controlled synthesis of hematite nanocrystals and their facet effects on gas sensing properties," Inorganic Chemistry, vol. 50, no. 20, pp. 10143-10151, 2011.

[51] J. A. Glasscock, P. R. F. Barnes, I. C. Plumb, and N. Savvides, "Enhancement of photoelectrochemical hydrogen production from hematite thin films by the introduction of Ti and Si," The Journal of Physical Chemistry C, vol. 111, no. 44, pp. 16477-16488, 2007.

[52] Y. H. Elbashar and H. A. Abd El-Ghany, "Optical spectroscopic analysis of Fe_2O_3 doped CuO containing phosphate glass," Optical and Quantum Electronics, vol. 49, no. 9, p. 310, 2017.

[53] S. S. Chiad, N. F. Habubi, W. H. Abass, and M. H. Abdul-Allah, "Effect of thickness on the optical and dispersion parameters of Cd0.4Se0.6 thin films," Journal of Optoelectronics and Advanced Materials, vol. 18, no. 9-10, pp. 822-826, 2016.

[54] R. Reveendran and M. A. Khadar, "Structural, optical and electrical properties of Cu doped α-Fe_2O_3 nanoparticles," Materials Chemistry and Physics, vol. 219, pp. 142-154, 2018.

[55] S. T. Navale, D. K. Bandgar, S. R. Nalage, G. D. Khuspe, M. A. Chougule, Y. D. Kolekar, S. Sen, and V. B. Patil, "Synthesis of Fe_2O_3 nanoparticles for nitrogen dioxide gas sensing applications," Ceramics International, vol. 39, pp. 6453-6460, 2013.

[56] R. Ben Ayed, M. Ajili, J. M. Garcia, A. Labidi, and N. K. Turki, "Physical properties investigation and gas sensing mechanism of Al: Fe_2O_3 thin films deposited by spray pyrolysis," Superlattices and Microstructures, vol. 129, pp. 91-104, 2019.

[57] R. Ben Ayed, M. Ajili, A. Thamri, N. T. Kamoun, and A. Abdelghani, "Substrate temperature effect on the crystal growth and optoelectronic properties of sprayed α-Fe_2O_3 thin films: application to gas sensor and novel photovoltaic solar cell structure," Materials Technology, vol. 33, pp. 769-783, 2018.

[58] Y. J. Park, K. M. A. Sobahan, and C. K. Hwangbo, "Optical and structural properties of Fe_2O_3 thin films prepared by ion-beam assisted deposition," Surface and Coatings Technology, vol. 203, pp. 2646-2650, 2009.

[59] A. A. Yadav, T. B. Deshmukh, R. V. Deshmukh, D. D. Patil, and U. J. Chavan, "Electrochemical supercapacitive performance of Hematite α-Fe_2O_3 thin films prepared by spray pyrolysis from non-aqueous medium," Thin Solid Films, vol. 616, pp. 351-358, 2016.

[60] K. M. Kwon et al., "α-Fe_2O_3 anchored on porous N doped carbon derived from green microalgae via spray pyrolysis as anode materials for lithium ion batteries," Journal of Industrial and Engineering Chemistry, vol. 69, pp. 39-47, 2019.

[61] Y. C. Chen, C. L. Kuo, and Y. K. Hsu, "Facile preparation of Zn-doped hematite thin film as photocathode for solar hydrogen generation," Journal of Alloys and Compounds, vol. 768, pp. 810-816, 2018.

[62] M. R. Belkhedkar, A. U. Ubale, Y. S. Sakhare, N. Zubair, and M. Musaddique, “Characterization and antibacterial activity of nanocrystalline Mn doped Fe_2O_3 thin films grown by successive ionic layer adsorption and reaction method,” Journal of the Association of Arab Universities for Basic and Applied Sciences, vol. 21, pp. 38-44, 2016.

[63] S. Riaz, A. Akbar, and S. Naseem, “Ferromagnetic Effects in Cr-Doped Fe_2O_3 thin Films,” IEEE Transactions on Magnetics, vol. 50, pp. 8-11, 2014.

[64] A. A. Khadayeir, R. I. Jasim, S. H. Jumaah, N. F. Habubi, and S. S. Chiad, “Influence of substrate temperature on physical properties of nanostructured ZnS thin films,” Journal of Physics: Conference Series, vol. 1664, no. 1, Art. no. 012009, 2020.

[65] Watanabe and H. Kozuka, “Photoanodic Properties of sol-gel-derived Fe_2O_3 thin films containing dispersed gold and silver particles,” The Journal of Physical Chemistry B, vol. 107, pp. 12713-12720, 2003.

[66] M. Lie, H. Fjellvåg, and A. Kjekshus, “Growth of Fe_2O_3 thin films by atomic layer deposition,” Thin Solid Films, vol. 488, pp. 74-81, 2005.

[67] S. D. Chavhan, S. V. Bagul, R. R. Ahire, N. G. Deshpande, A. A. Sagade, Y. G. Gudage, and R. Sharma, “Study of Fe_2O_3 thin films,” Journal of Alloys and Compounds, vol. 436, pp. 400-406, 2007.

[68] T. Wang, D. Huang, Z. Yang, S. Xu, G. He, X. Li, N. Hu, G. Yin, D. He, and L. Zhang, “A review on graphene-based gas/vapor sensors with unique properties and potential applications,” Sensors and Actuators B: Chemical, vol. 288, no. 1, pp. 110-116, 2019.

[69] N. M. Ahmed, M. Z. Mat Jafri, and A. F. Omar, “Structural and morphological study of Li-doped Fe_2O_3 thin films for sensing application,” Thin Solid Films, vol. 780, no. 1, Art. no. 139987, 2023.